Article:
Narata, A.P., Moura, F., Larrabide, I. et al. (7 more authors) (2020) Role of distal cerebral vasculature in vessel constriction after aneurysm treatment with flow diverter stents. Journal of NeuroInterventional Surgery. ISSN 1759-8478

https://doi.org/10.1136/neurintsurg-2019-015447

Journal of
NeuroInterventional Surgery

The role of distal cerebral vasculature in vessel constriction after aneurysm treatment with flow-diverter stents

Journal:	*Journal of NeuroInterventional Surgery*
Manuscript ID	neurintsurg-2019-015447.R1
Article Type:	Original research
Keywords:	Blood Flow, Aneurysm, Flow Diverter, Ultrasound

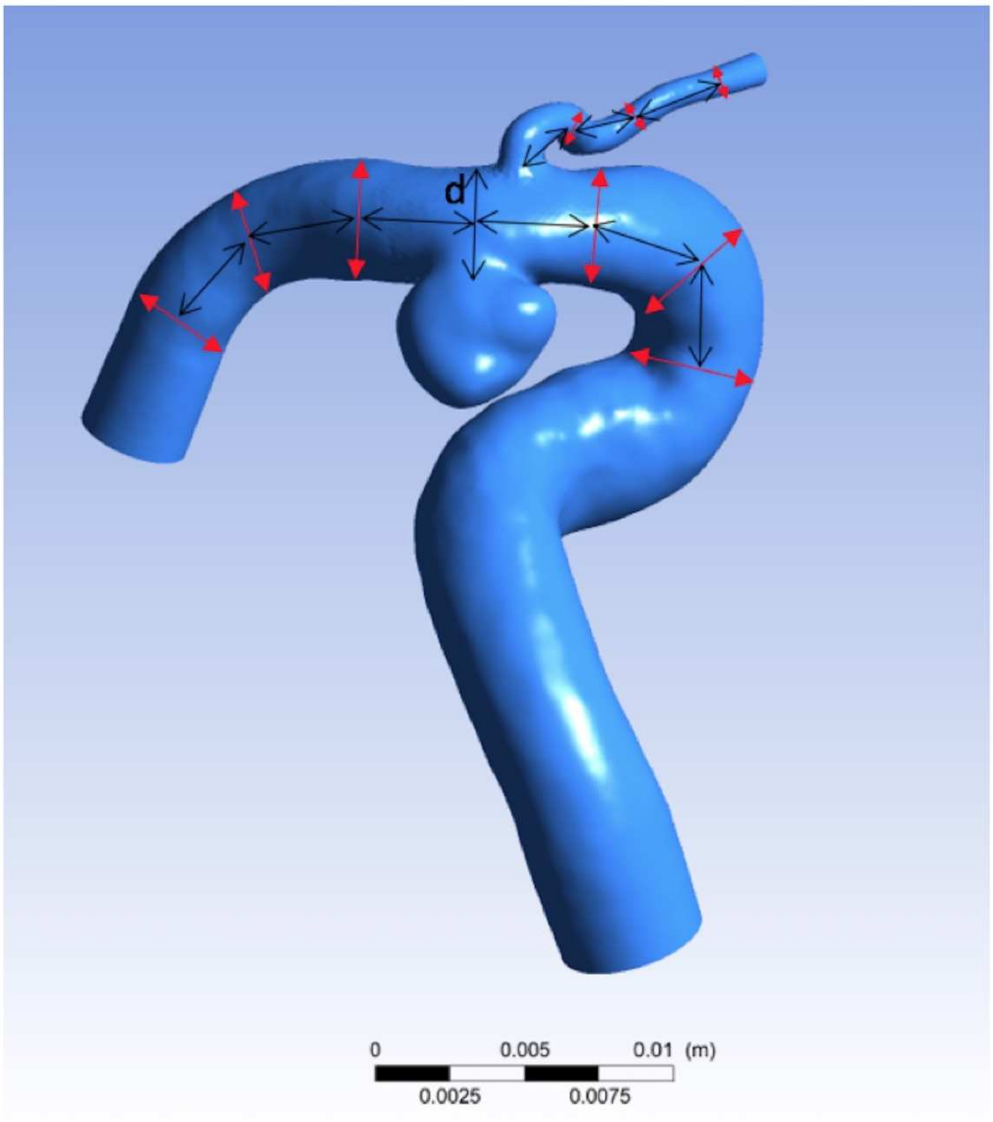

Fig 1 (online suppl.) Measurement protocol followed to extract bifurcation-vessel diameter values. Red arrows indicate approximate locations of measurements, black arrows indicate approximate distances (d= parent vessel lumen diameter at aneurysm location) among consecutive measurements locations. A similar measurement protocol was followed for aneurysms at other locations.

127x148mm (600 x 600 DPI)

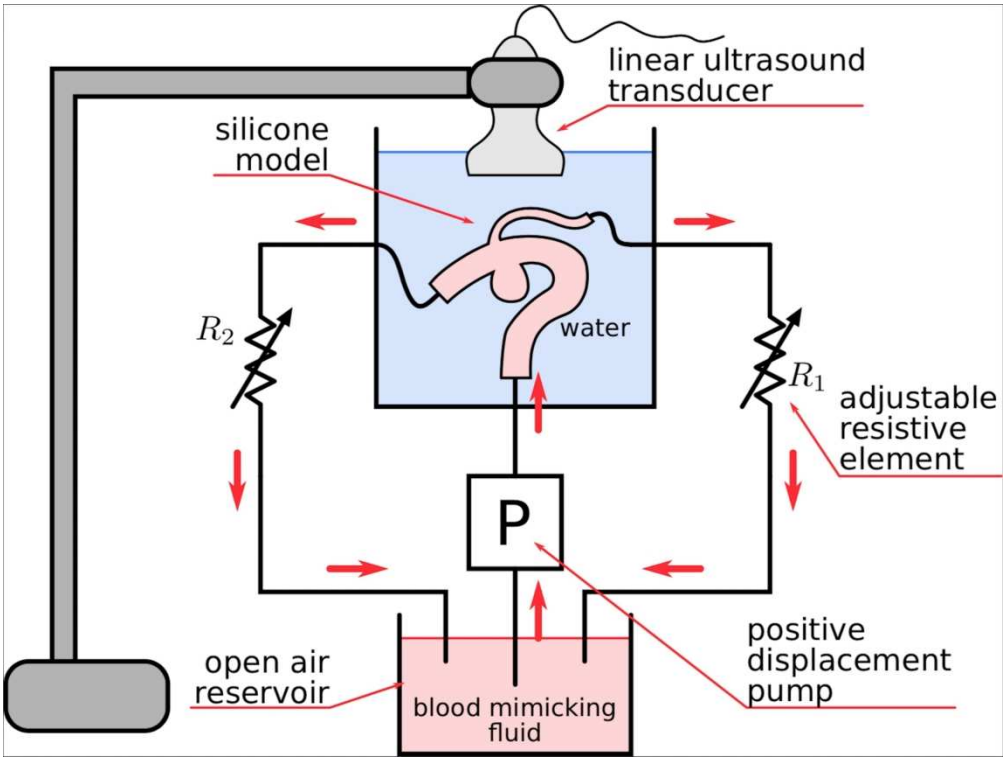

Fig 2 (online suppl.) Closed loop circuit filled with ultrasound compatible blood mimicking fluid and connected to a programmable pump. Silicone models were produced based on patient-specific geometry.

127x95mm (600 x 600 DPI)

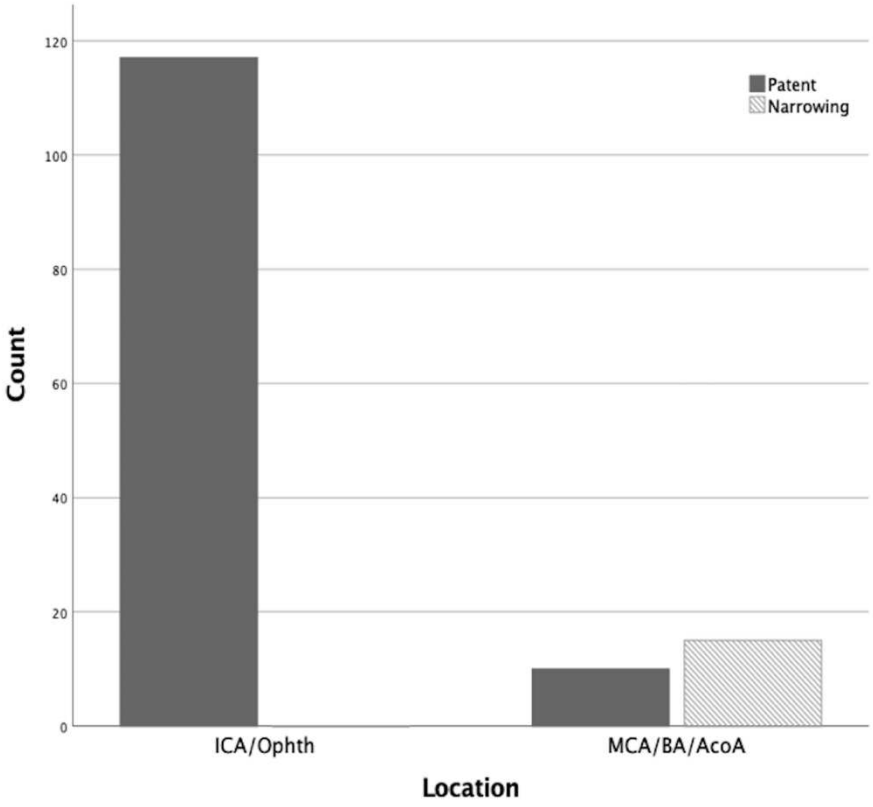

Fig 3 (online suppl.) Graph showing distribution of vessel narrowing (shadowed grey) and patent (dark grey) jailed vessels subgroup by location of aneurysm in internal carotid artery (ICA)/ophthalmic artery (OphthA) (left) and in middle cerebral artery (MCA)/basilar artery (BA)/anterior communicating artery (AcomA) bifurcations (right).

126x108mm (600 x 600 DPI)

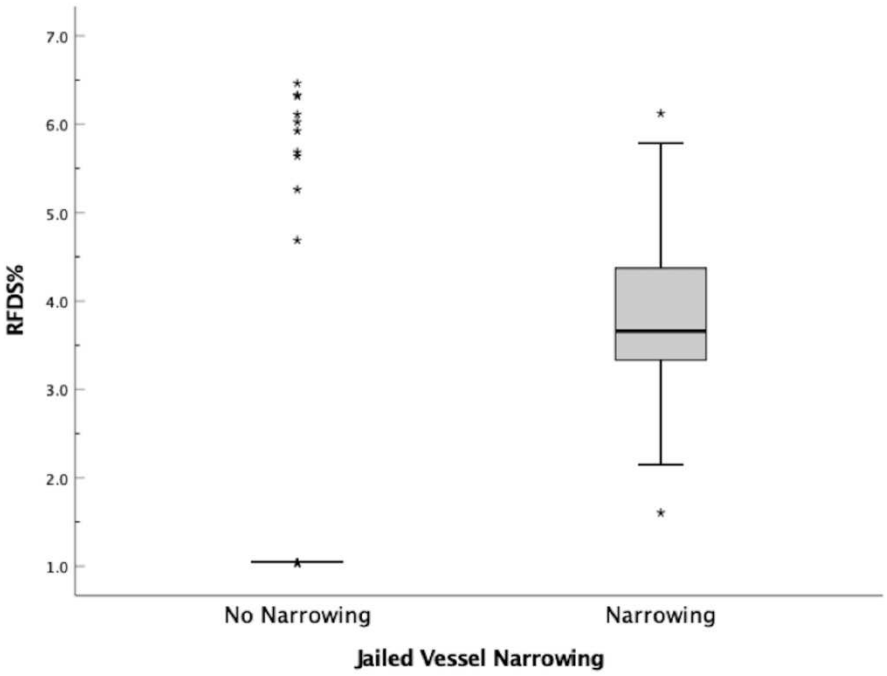

Fig 4 Whisker plots showing distribution of FDS resistance to flow as a percentage of overall jailed vessel vascular resistance (RFDS%) for datasets showing jailed vessel patency (left, mean = 1.048, lower bound = 1.046, upper bound = 1.05) and narrowing (right, mean =3.7, lower bound = 3.33, upper bound = 4.5). Solid lines within the boxes indicate median values. Each boxplot describes first quartile values (bottom black line), median values (middle black line), and third quartile values (top black line). Error bars (whiskers) show minimum (bottom black bar) and maximum (top black bar) values. Stars denote outliers identified by using the maximum normed residual test.

127x97mm (600 x 600 DPI)

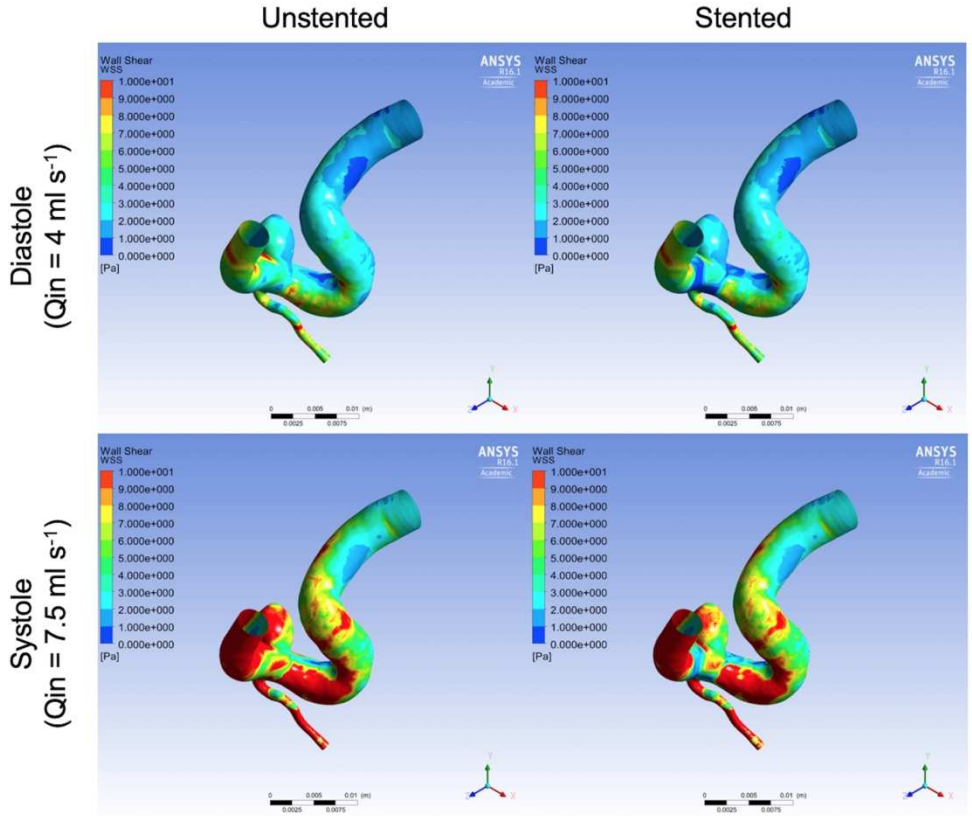

Fig 5 WSS contours at peak systole (Qin= 7.5 ml s-1) for the unstented (top left) and stented (top right) models. WSS contours at end diastole (Qin= 4 ml s-1) for the unstented (bottom left) and stented (bottom right) models.

104x86mm (600 x 600 DPI)

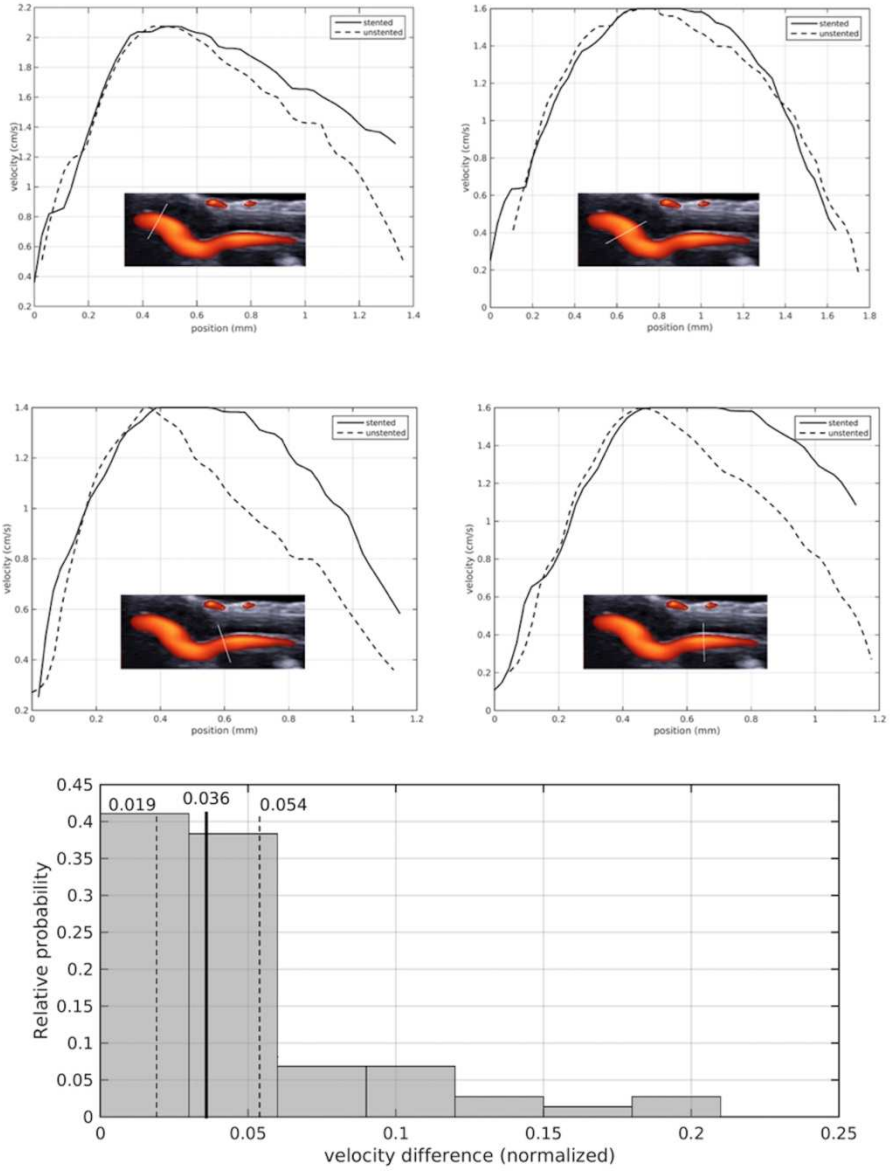

Fig 6 (Top) Velocity profile PD-US measurements (for Qin= 4 ml s-1) for the unstented (dashed line) and stented (solid line) replicas. The in-box images show the PD-US images and the locations along the OphthA where the velocity measurements were extracted (flow in OphthA directed left-to-right in in-box images). (Bottom) Normalized velocity discrepancy obtained from 75 measurements taken at different locations along the OphthA. The continuous line indicates the median value and the dashed lines represent quartiles Q1 and Q3.

101x128mm (600 x 600 DPI)

Fig 1 (online suppl.) Measurement protocol followed to extract bifurcation-vessel diameter values. Red arrows indicate approximate locations of measurements, black arrows indicate approximate distances (d= parent vessel lumen diameter at aneurysm location) among consecutive measurements locations. A similar measurement protocol was followed for aneurysms at other locations.

Fig 2 (online suppl.) Closed loop circuit filled with ultrasound compatible blood mimicking fluid and connected to a programmable pump. Silicone models were produced based on patient-specific geometry.

Fig 3 (online suppl.) Graph showing distribution of vessel narrowing (shadowed grey) and patent (dark grey) jailed vessels subgroup by location of aneurysm in internal carotid artery (ICA)/ophthalmic artery (OphthA) (left) and in middle cerebral artery (MCA)/basilar artery (BA)/anterior communicating artery (AcomA) bifurcations (right).

Fig 4 Whisker plots showing distribution of FDS resistance to flow as a percentage of overall jailed vessel vascular resistance (RFDS%) for datasets showing jailed vessel patency (left, mean = 1.048, lower bound = 1.046, upper bound = 1.05) and narrowing (right, mean =3.7, lower bound = 3.33, upper bound = 4.5). Solid lines within the boxes indicate median values. Each boxplot describes first quartile values (bottom black line), median values (middle black line), and third quartile values (top black line). Error bars (whiskers) show minimum (bottom black bar) and maximum (top black bar) values. Stars denote outliers identified by using the maximum normed residual test.

Fig 5 WSS contours at peak systole (Q_{in}= 7.5 ml s^{-1}) for the unstented (top left) and stented (top right) models. WSS contours at end diastole (Qin= 4 ml s-1) for the unstented (bottom left) and stented (bottom right) models.

Fig 6 (Top) Velocity profile PD-US measurements (for Qin= 4 ml s-1) for the unstented (dashed line) and stented (solid line) replicas. The in-box images show the PD-US images and the locations along the OphthA where the velocity measurements were extracted (flow in OphthA directed left-to-right in in-box images). (Bottom) Normalized velocity discrepancy obtained from 75 measurements taken at different locations along the OphthA. The continuous line indicates the median value and the dashed lines represent quartiles Q1 and Q3.

Table 2 Quantification of FDS-induced changes to haemodynamic variables extracted from OphthA bifurcation at peak systole (peak) and end diastole (dia). Avg WSS is the space-averaged WSS extracted from the OphthA. ICA and Ophth outflow are the volumetric flow rates calculated at the outlet of the ICA and OphthA, respectivelty.

	Unstented [peak/dia]	*Stended* [peak/dia]	*Diff* [peak/dia]	*%Diff* [peak/dia]
Avg WSS [Pa]	11.56/5.30	10.98/5.04	-0.58/-0.26	-5.0/-4.7
ICA outflow [ml/s]	7.20/3.80	7.19/3.82	-0.01/-0.02	0.1/0.5
Ophth outflow [ml/s]	0.38/0.20	0.38/0.201	0.0/0.001	0.0/0.5

Dataset	Location	J-Ves Narrowing	J-Vess Diam [mm]	J-Vess R [mmHg s ml^-1]	Periph R [mmHg s ml^-1]	R_{FDS} [mmHg s ml^-1]	$\%R_{FDS}$
1	ICA	NO	1.09	8	470	5	1.04
2	ICA	NO	1.05	10	470	5	1.04
3	ICA	NO	1.08	9	470	5	1.04
4	ICA	NO	1.07	9	470	5	1.04
5	ICA	NO	1.08	9	470	5	1.04
6	ICA	NO	1.16	6	470	5	1.05
7	ICA	NO	1.07	9	470	5	1.04
8	ICA	NO	1.24	5	470	5	1.05
9	ICA	NO	1.06	9	470	5	1.04
10	ICA	NO	1.13	7	470	5	1.05
11	ICA	NO	1.23	5	470	5	1.05
12	ICA	NO	1.09	8	470	5	1.05
13	ICA	NO	1.30	4	470	5	1.05
14	ICA	NO	1.14	7	470	5	1.05
15	ICA	NO	1.11	8	470	5	1.05
16	ICA	NO	1.13	7	470	5	1.05
17	ICA	NO	1.17	6	470	5	1.05
18	ICA	NO	1.21	6	470	5	1.05
19	ICA	NO	1.17	6	470	5	1.05
20	ICA	NO	1.11	8	470	5	1.05
21	ICA	NO	1.15	7	470	5	1.05
22	ICA	NO	1.15	7	470	5	1.05
23	ICA	NO	1.27	5	470	5	1.05
24	ICA	NO	1.15	7	470	5	1.05
25	ICA	NO	1.19	6	470	5	1.05
26	ICA	NO	0.98	13	470	5	1.04
27	ICA	NO	1.10	8	470	5	1.05
28	ICA	NO	1.16	6	470	5	1.05
29	ICA	NO	1.16	7	470	5	1.05
30	ICA	NO	1.19	6	470	5	1.05
31	ICA	NO	1.10	8	470	5	1.05
32	ICA	NO	1.18	6	470	5	1.05
33	ICA	NO	1.14	7	470	5	1.05
34	ICA	NO	1.01	11	470	5	1.04

Table 1 ***Demographic constitution and anatomical data of patients' population. J-Vess Diam = jailed vessel diameter, J-Vess R = jailed vessel vascular resistance, Periph R = peripheral resistance, R_{FDS}= FDS-induced resistance to flow, % R_{FDS}= FDS-induced resistance to flow given as a percentage of overall resistance (FDS plus vascular plus peripheral).***

35	ICA	NO	1.18	6	470	5	1.05
36	ICA	NO	1.17	6	470	5	1.05
37	ICA	NO	1.12	7	470	5	1.05
38	ICA	NO	1.30	4	470	5	1.05
39	ICA	NO	1.14	7	470	5	1.05
40	ICA	NO	1.22	5	470	5	1.05
41	ICA	NO	1.27	5	470	5	1.05
42	ICA	NO	1.07	9	470	5	1.04
43	ICA	NO	1.22	5	470	5	1.05
44	ICA	NO	1.15	7	470	5	1.05
45	ICA	NO	1.23	5	470	5	1.05
46	ICA	NO	1.26	5	470	5	1.05
47	ICA	NO	1.13	7	470	5	1.05
48	ICA	NO	1.08	9	470	5	1.04
49	ICA	NO	1.25	5	470	5	1.05
50	ICA	NO	1.10	8	470	5	1.05
51	ICA	NO	1.25	5	470	5	1.05
52	ICA	NO	1.13	7	470	5	1.05
53	ICA	NO	1.11	8	470	5	1.05
54	ICA	NO	1.10	8	470	5	1.05
55	ICA	NO	1.19	6	470	5	1.05
56	ICA	NO	1.05	10	470	5	1.04
57	ICA	NO	1.12	8	470	5	1.05
58	ICA	NO	1.15	7	470	5	1.05
59	ICA	NO	1.12	8	470	5	1.05
60	ICA	NO	1.09	8	470	5	1.04
61	ICA	NO	1.20	6	470	5	1.05
62	ICA	NO	1.13	7	470	5	1.05
63	ICA	NO	1.17	6	470	5	1.05
64	ICA	NO	1.09	8	470	5	1.05
65	ICA	NO	1.14	7	470	5	1.05
66	ICA	NO	1.00	12	470	5	1.04
67	ICA	NO	1.13	7	470	5	1.05
68	ICA	NO	1.12	8	470	5	1.05
69	ICA	NO	1.14	7	470	5	1.05
70	ICA	NO	1.16	6	470	5	1.05
71	ICA	NO	1.11	8	470	5	1.05
72	ICA	NO	1.12	7	470	5	1.05
73	ICA	NO	1.11	8	470	5	1.05
74	ICA	NO	1.18	6	470	5	1.05
75	ICA	NO	1.13	7	470	5	1.05
76	ICA	NO	1.10	8	470	5	1.05

77	ICA	NO	1.13	7	470	5	1.05
78	ICA	NO	1.05	10	470	5	1.04
79	ICA	NO	1.17	6	470	5	1.05
80	ICA	NO	1.12	7	470	5	1.05
81	ICA	NO	1.14	7	470	5	1.05
82	ICA	NO	1.20	6	470	5	1.05
83	ICA	NO	1.14	7	470	5	1.05
84	ICA	NO	1.05	10	470	5	1.04
85	ICA	NO	1.19	6	470	5	1.05
86	ICA	NO	1.05	10	470	5	1.04
87	ICA	NO	1.14	7	470	5	1.05
88	ICA	NO	1.13	7	470	5	1.05
89	ICA	NO	1.15	7	470	5	1.05
90	ICA	NO	1.05	10	470	5	1.04
91	ICA	NO	1.20	6	470	5	1.05
92	ICA	NO	1.17	6	470	5	1.05
93	ICA	NO	1.12	8	470	5	1.05
94	ICA	NO	1.13	7	470	5	1.05
95	ICA	NO	1.03	11	470	5	1.04
96	ICA	NO	1.16	7	470	5	1.05
97	ICA	NO	1.13	7	470	5	1.05
98	ICA	NO	1.11	8	470	5	1.05
99	ICA	NO	1.11	8	470	5	1.05
100	ICA	NO	1.07	9	470	5	1.04
101	ICA	NO	1.12	8	470	5	1.05
102	ICA	NO	1.17	6	470	5	1.05
103	ICA	NO	1.03	10	470	5	1.04
104	ICA	NO	1.13	7	470	5	1.05
105	ICA	NO	1.16	6	470	5	1.05
106	ICA	NO	1.09	8	470	5	1.05
107	ICA	NO	1.13	7	470	5	1.05
108	ICA	NO	1.17	6	470	5	1.05
109	ICA	NO	1.17	6	470	5	1.05
110	ICA	NO	1.13	7	470	5	1.05
111	ICA	NO	1.14	7	470	5	1.05
112	ICA	NO	1.17	6	470	5	1.05
113	ICA	NO	1.02	11	470	5	1.04
114	ICA	NO	1.13	7	470	5	1.05
115	ICA	NO	1.11	8	470	5	1.05
116	ICA	NO	1.15	7	470	5	1.05
117	ICA	NO	1.11	8	470	5	1.05
118	MCA	YES	1.05	62	75	5	3.66

119	ACOM	YES	1.05	62	75	5	3.66
120	MCA	YES	1.6	11	75	5	5.79
121	MCA	YES	1.05	62	75	5	3.66
122	BA	YES	1.15	43	75	5	4.24
123	MCA	YES	1.04	64	75	5	3.60
124	MCA	NO	1.55	13	75	5	5.68
125	MCA	NO	1.53	14	75	5	5.64
126	MCA	YES	1.2	36	75	5	4.50
127	MCA	NO	2.06	4	75	5	6.32
128	MCA	NO	2.37	2	75	5	6.46
129	MCA	YES	0.83	158	75	5	2.15
130	MCA	NO	1.82	7	75	5	6.11
131	BA	YES	0.75	237	75	5	1.60
132	MCA	YES	1.83	7	75	5	6.12
133	BA	NO	2.08	4	75	5	6.33
134	BA	NO	1.39	20	75	5	5.26
135	MCA	YES	1.04	64	75	5	3.60
136	BA	YES	0.96	88	75	5	3.06
137	BA	NO	1.24	32	75	5	4.69
138	MCA	NO	1.68	9	75	5	5.92
139	MCA	YES	1.1	51	75	5	3.96
140	MCA	YES	1.6	11	75	5	5.79
141	ACOM	NO	1.75	8	75	5	6.03
142	MCA	YES	0.88	125	75	5	2.50

The role of peripheral vasculature in vessel constriction after aneurysm treatment with flow-diverter stents

Abstract

Background Treatment of intracranial aneurysms with flow diverter stents (FDS) can lead to calibre changes of jailed vessels. The reason some branches remain unchanged and others are affected by narrowing remains unknown.

Objective This study investigates the influence of resistance to flow from distal vasculature on stent-induced haemodynamic modifications affecting bifurcating vessels.

Materials and methods Radiological images and demographic data were acquired for 142 aneurysms treated with FDS. Vascular resistance values were estimated from patient-specific anatomical data. Correlation analysis was used to identify correspondence between anatomical data and clinical outcome. Computational Fluid Dynamics was performed on a typical patient-specific model to evaluate FDS-specific influence on flow. Relevant haemodynamic variables along the bifurcating vessels were quantitatively analysed and validated with *in vitro* data obtained using power Doppler ultrasound.

Results Statistical analysis showed a correlation between clinical outcome and FDS resistance to flow considering overall jailed-vessel vascular resistance ($r=0.5$, $p<0.001$). Computational predictions of blood flow showed that haemodynamics is minimally affected by FDS treatment in the OphthA.

Conclusions Jailed vessels are affected by narrowing when resistance to flow from the FDS constitutes a larger proportion of overall vessel resistance to flow. This knowledge may contribute to better understanding of intracranial hemodynamic after FDS procedure and reinforce indications of flow diversion in the treatment of intracranial aneurysms.

INTRODUCTION

Flow diverter stent (FDS) procedures for proximal internal carotid artery (ICA) aneurysms are a frequent treatment with high aneurysm obliteration rates. Neurological impairment remains relatively low considering that FDS covers not only the aneurysm neck but also side wall arteries like ophthalmic (OphthA) and anterior choroidal arteries [1]–[3], that seem to be less affected than bifurcating arteries when jailed by FDS [4]–[12]. Narrowing and occlusion are a frequent event after FDS procedure for middle cerebral artery (MCA) and some anterior cerebral artery (ACA) bifurcation aneurysms (MCA and ACA bifurcations without opposite A1) and anatomic parameters could be involved in hemodynamic changes that affect the vessel wall. Asymmetry of branches, hemodynamic alterations and clinical outcome after treatment with FDS for bifurcation aneurysms have been correlated in a study that identified an anatomical threshold of the daughter vessel diameter ratio (0.7) below which FDS-induced alterations of volumetric flow rates and significant changes in wall shear stress (WSS) correlate to poor clinical outcome[13]. It is difficult to apply this theory in the context of proximal ICA aneurysms considering that the ratio between OphthA and ICA are lower than 0.7, and jailed OphthA remains mostly patent. Iosif and colleagues evaluated the presence of collaterals converging to the same territory of the jailed artery to explain the narrowing process, however this hypothesis does not explain OphthA permeability after FDS procedures as collaterals are often present in this territory too [14].

In an attempt to explain this phenomenon, Cebral et al.[15] proposed the role of high peripheral vascular resistance (R_{PER}) as the most significant factor affecting hemodynamics and possibly vessel calibre changes after FDS treatment. Their study showed that computational estimations of blood flow patterns in the jailed arteries are only

minimally affected by the small perturbation imposed by the FDS and mainly influenced by the much larger resistance to flow imposed by the peripheral bed distal to these small arteries. Blood flow distribution throughout the cardiovascular system is highly influenced by R_{PER}, which can be described as the viscous impediment to blood flow in a vessel as described by the Hagen-Poiseuille relationship that links pressure to flow [16]. This relationship shows that resistance, or impediment to flow, increases with higher values of blood viscosity (hematocrit), vessel length and smaller vessel radii.

The aim of this study is to perform a quantitative estimation of the factors affecting hemodynamics of FDS-jailed arteries, with a focus on the quantification of the impediment to flow from the FDS (R_{FDS}) in relation to the overall artery resistance (R_{TOT}) to flow, and for a larger cohort of datasets. The study also includes an experimental validation of our theoretical and numerical observations using power doppler-ultrasound (PD-US).

MATERIALS AND METHODS

The hypothesis of this study is that clinical outcome and FDS-induced hemodynamic alterations depend on the relative significance of R_{FDS} to flow with respect to overall artery resistance ($R_{TOT=}$ R_{FDS}+R_{JV}+R_{PER}) in the jailed artery (local jailed artery resistance= R_{JV}). The methodology of this study was developed to test this hypothesis and organized within 3 different phases: Phase I=analysis of clinical data (radiological and demographic) for estimation of vascular resistances and possible associations with clinical outcomes; Phase II=patient-specific computational fluid dynamics (CFD) analysis of flow through a typical OphthA aneurysm to analyze and illustrate the effect of R_{FDS} to flow at a location normally

less affected by vessel narrowing; Phase III=validation of numerical predictions through experimental analysis.

Phase I

Clinical data from 142 patients were retrospectively collected upon appropriate ethical approval and patient consent. Bifurcation aneurysms from middle cerebral artery (MCA), basilar artery with hypoplasia of posterior communicating artery and anterior communicating artery aneurysms with agenesis of contra-lateral anterior cerebral artery and treated with FDS between December 2010 and December 2015 were included (25 aneurysms from 25 patients). OphthA aneurysms data were collected from December 2014 to December 2017 (117 aneurysms from 117 patients). All patients included had 3D-angiography prior to FDS positioning and at 3-6 months follow-up. Images were acquired using a biplane X-ray system (General Electric Healthcare Innova IGS 650, Marlbourough, Massachusetts, USA) and were obtained during a 240 degrees rotation for a duration of 5 seconds and for a total of 244 projections. This resulted in a 3D volume dataset of 512x512x512 voxels covering a field of view of 116 mm.

Table 1 (online suppl.) illustrates the demographic constitution of the data together with jailed-vessel outcomes, anatomic information (lumen diameter) and estimations of local resistance to flow. Resistances were calculated from jailed-vessel patient-specific diameter values using Hagen-Poiseuille's theory $R = 8 \mu L / (\pi r^4)$, where μ=*0.0035 Pa s* is whole blood viscosity, *L* is vessel length and *r* is lumen radius. Typical values of vessel length for jailed arteries and R_{PER} values were taken from Reymond *e*t al.[17]. Three vessel diameter values were taken from radiological images by two fully trained neuroradiologists along the

vessels of each bifurcating branch (Fig 1, online suppl.), reporting only its arithmetic average value and their standard deviation to quantify interobserver variability. OsiriX was used to measure vessel diameters from 2D acquisitions by digital subtraction angiography and 3D-angiography images. 2-way, mixed intra-class correlation coefficients was used to assess the reliability of measurements with 95% confidence interval. 2-tailed Pearson correlation analysis was performed to identify associations between clinical outcome, anatomical data and estimation of vascular and relative R_{FDS} to flow. Although normally a probability value of $p < 0.05$ is sufficient to test correlation significance, for our relatively small cohort, we wanted to test our hypothesis to a more stringent significant region and decided to set 0.01 as probability value threshold.

Phase II

For the patient-specific CFD analysis, an aneurysm located at OphthA segment was selected. Medical image segmentation and surface reconstruction were performed using the @neurIST computational toolchain[18]. Blender® was used for removal of artefacts and further surface mesh refinements. FDS was deployed virtually, in accordance with clinical procedures, and using the process described by Larrabide et al [19]. The FDS model represents a typical Surpass FDS (Stryker, Kalamazoo, MI, USA) of 4 mm diameter with 72 wires. For the same patient-specific geometry we run several analyses, with and without stent, and for different flow conditions.

The equations governing the physics of steady laminar flow were solved by using ANSYS CFX (ANSYS, Canonsburg, Pennsylvania). Blood was assumed incompressible (density ρ = 1050 kg m^{-3}) and Newtonian (viscosity μ = 0.0035 Pa s). Appropriateness of modelling approaches and accuracy of the numerical solutions was ensured by adopting methodologies

already reported in the literature[13], [18], [20], [21]. The mesh used for the unstented model comprised approximately 0.8 million nodes (4 million nodes for stented model) and 2.7 million elements (19 million elements for stented model), resulting in a mesh volumetric density of 2.7 thousand elements mm^{-3} (19 thousand el. mm^{-3} for stented model). Typical volumetric flow rates, time-averaged along the cardiac cycle, were imposed at inlet in the form of a fully developed parabolic velocity profile to mimic peak systolic (Q_{in} = 4 ml s^{-1}) and end diastolic (Q_{in} = 7.5 ml s^{-1}) conditions. Outlet boundary conditions were imposed by mimicking typical resistance to flow imposed by the peripheral networks distal to the ICA and OphthA [22]. R_{PER} at distal ICA outlet boundary was set to R_{ICA} = 25 mmHg s mL^{-1}, whereas resistances at the OphthA outlet were set to R_{OphthA} = 470 mmHg s mL^{-1}. CFD analysis and results were also used to obtain values of resistance to flow caused by the FDS by extracting values of pressure drops and flow across the wires and calculating resistance as $R=\Delta P/Q$, where ΔP is the pressure drop measured across the stent wires, and Q the flow rate across the same location.

Phase III

CFD data were validated via PD-US measurements from life-size silicone replicas purposely produced for the study. Two silicone replicas of the geometry used in the CFD analysis were produced. The difference between the surfaces of the produced replicas and their target STL surfaces was evaluated quantitatively using a position error index method [23]. This resulted in a median value for the distribution of position errors across the surface mesh below 70µm. One of the replicas received an FDS Surpass (Stryker, Kalamazoo, MI, USA) 4mm diameter by 20mm length with 72 wires, deployed by a senior intervention neuroradiologist (APN) carefully placing the stent to match with CFD model. Both replicas

were connected to a closed loop circuit filled with ultrasound compatible blood mimicking fluid and connected to a programmable pump (CompuFlow 1000, Shelley Medical Imaging Technologies, Toronto, Canada).

An Ultrasound System (Aixplorer® Multiwave Supersonic Imagine, S.A.; Aix-en-Provence, France) equipped with a 256-element (SL15–4) 7.5-MHz linear-array transducer was used to take PD-US measurements of velocity magnitude along the OphthA from both replicas. Velocities profiles were extracted from PD-US along the OphthA and compared to identify FDS-induced changes and validation of CFD data (Fig 2, online suppl.).

RESULTS

Phase I: Clinical data analysis results

Reports of the incidence of vessel narrowing per location, showing a higher incidence of clinical complications for vessels jailed by the FDS in bifurcating aneurysms and no complications for FDS-treatment of aneurysms at OphthA location at 3 months follow up are shown in Fig 3 (online suppl.). The intra-class correlation and Pearson correlation performed to assess the reliability of the anatomical measurements showed high interclass correlation coefficient (ICC=0.97, CI 95%, lower bound = 0.95, upper bound = 0.998, $p<0.0001$ and Pearson Correlation Coefficient $r=0.743$, $p<0.0001$). Mortality was not considered as only patients with control at 3 months follow-up were included.

Box-plots graphs in Fig 4 show relation between R_{FDS} to flow and R_{TOT} ($R_{FDS}+R_{JV}+R_{PER}$) for cases showing patency (no narrowing) and narrowing of the jailed vessel. The graphs clearly indicate that those cases where median R_{FDS} to flow is low compared with R_{TOT} are also the cases presenting no complications (Fig 4, patent group, mean=1.05). On the

contrary, cases with relatively higher R_{FDS} to flow are also the cases presenting vessel narrowing (Fig 4, narrowing group, mean=3.6). This correlation is statistically significant as showed by the Pearson correlation analysis reporting a Pearson correlation coefficient of r=0.5 ($p<0.0001$).

Phase II: CFD analysis

The CFD results obtained for the patient-specific analysis of flow through an OphthA showed that FDS-induced changes mostly affect values within the aneurysm sac and parent vessel, and not visibly affect values in the jailed OphthA (Table 2 and Fig 5). Table 2 reports FDS-induced changes on flow redistributions (ICA and OphthA outflow) at peak systole (peak) and end diastole (dia), showing values below 0.5%. FDS-induced changes on WSS space-averaged across the OphthA show reduction in values below 5%. In accordance with the quantitative values reported in Table 2, Fig 5 shows the spatial distribution of WSS magnitude across the patient-specific model, indicating that FDS-induced changes mostly affect values within the aneurysm sac and parent vessel, and not visibly affect values in the jailed OphthA, both at peak systole and end diastole.

Phase III: Validation results

Velocity profiles from both replicas were obtained from PD-US measurements. Profiles at the same positions along the OphthA were extracted and the changes were quantified using a normalized discrepancy index $D = \frac{|V_{unstented} - V_{stented}|}{\max(V_{unstented})}$. Profiles at four different positions are presented in Fig 6. The discrepancy index, D, was computed up to 0.4mm deep into the vessel due to limitations in accuracy in the PD-US approach. Fig 6 presents the histogram of the discrepancy D (N=75 samples). The median of the discrepancy

is 3.6%, in agreement with CFD analysis. The measurements corroborate that FDS does not induce significant changes to the flow in the jailed OphthA.

DISCUSSION

The aim of the study was to investigate, for a cohort of 142 aneurysm datasets, the role of resistance to flow in the context of flow changes induced by FDS treatment that may relate to vessel narrowing/occlusion in a subacute phase. The effect of FDS on flow distribution at symmetric and asymmetric bifurcations was studied in the past, but this was contrasted to a small number of cases (25) which was not enough to explain the changes in vessel diameter [13].

The statistical analysis results of this study showed significant correlations between flow resistance attributed to the presence of the FDS and vessel narrowing at follow-up. Analysis of R_{FDS} were considered as values relative to the overall resistance to flow, R_{TOT}, encountered by the viscous flow of blood through the jailed vessel and distal R_{PER}. R_{FDS} estimated from the CFD simulations in the OphthA were almost negligible (1%) when compared to R_{TOT}, mostly due to a large R_{PER}. Correlation was found with the CFD analysis, which showed that WSS values and flow redistributions were only marginally affected by the presence of the stent (changes ranging from 0 to 5%). Experimental data obtained with PD-US on a silicon replica of a typical OpthA found similar alterations to flow (median value = 3.6%). The importance of R_{PER} in side-wall branches after stenting was also highlighted by Appanaboyinaa et al.[24] in their analysis of blood flow in three patient-specific models.

The study presented here goes one step further by estimating not only R_{PER} but all resistances encountered by blood as it flows through the jailed vessels and how these relate to the additional resistance to flow imposed by the stent. For these calculations lumen caliber data were derived from imaging data of 142 datasets. It is well established that flow distribution and WSS are heavily dominated by vessel anatomy and the viscous nature of blood as smaller vessels, such as the OphthA, will oppose higher resistance to flow than relatively larger vessels like MCA branches. So the presence of a FDS will not affect the resistance in the OphthA because it is already high.

The distribution of R_{FDS} to flow as a percentage of R_{TOT} between cases showing jailed vessel patency and narrowing/occlusion was much higher (2 to 6 fold) in this latter group. In the not narrowing cases, a series of outliers ranging from 4.5 to 6.5 fold the R_{FDS}% can be observed. This can be explained by the fact that the data have been collected from follow up images. The narrowing is a biological response to a change in flow, which is not instantaneous and might take different times depending on the physiological condition of the patient, or might not happen at all.

This study has some limitations that should be highlighted. Some of the data used to compute vascular resistance (eq. 2) were typical values from the literature (i.e. blood viscosity, vessel length), and vessel tortuosity and its effect on flow resistance was not considered. This might result in some discrepancies between our estimations and the real values. However, these discrepancies could be negligible as the most influential parameter to flow resistance (lumen radius) was patient-specific. CFD simplifying assumptions included: Newtonian, incompressible and stationary fluid, which were adopted following previous results in the literature, where it was observed that CFD variables like velocity and WSS resulting from steady state simulations were equivalent to averaging the same variables over

the cardiac cycle for a transient simulation [25]. In this study we are assessing pressure drop, velocity, mass inflow, and WSS at specific locations for a period of time that is considerably longer than a single cardiac cycle. Therefore, the use of steady state instead of transient CFD simulations is safe, with additional benefit of a considerable computational time reduction. The non-Newtonian effect on the above mentioned variables is observed for shear rates at a much lower regime than considered in this study [26]. Vascular remodeling is a complex biological process strongly related to fluid-wall mechanics and their interaction. The study of vascular wall remodeling and wall change over time has been modelled computationally in the past with promising results [27]. Still, the complexity of determining personalized wall properties and associated mechanobiological parameters makes the use of such models non practical in the cases studied, which is a limitation. The link of such models to local hemodynamic parameters (WSS) that might induce vascular changes and remodeling should be a subject of future studies, to help further understand the reasons for these changes at follow-up.

CONCLUSIONS

Observations of FDS procedures in some bifurcation aneurysms and side-wall arteries seem to have different arterial narrowing/occlusion rates of the jailed arteries by the stent. This study identified statistically significant correlations between flow resistance and vessel narrowing that could explain large patency rates in OphthA in a cohort of 142 aneurysms. This was further supported by a numerical and experimental analysis of blood flow through a typical OphthA that were used to identify and illustrate the mechanisms explaining these correlations. A complete understanding of the phenomena at play will only be possible when mechanobiological pathways linking hemodynamics alterations to endothelial cells and

arterial wall response (vasoconstriction or remodeling) are also considered. It is necessary a better understanding of intracranial hemodynamic after FDS procedure to reinforce indications of flow diversion in the treatment of intracranial aneurysms.

REFERENCES

[1] W. Brinjikji, M. H. Murad, G. Lanzino, H. J. Cloft, and D. F. Kallmes, "Endovascular treatment of intracranial aneurysms with flow diverters: A meta-analysis," *Stroke*. 2013.

[2] P. Jabbour *et al.*, "The pipeline embolization device: Learning curve and predictors of complications and aneurysm obliteration," *Neurosurgery*, 2013.

[3] A. P. Narata *et al.*, "Dual Antiplatelet Therapy Combining Aspirin and Ticagrelor for Intracranial Stenting Procedures: A Retrospective Single Center Study of 154 Consecutive Patients With Unruptured Aneurysms," *Neurosurgery*, 2019.

[4] C. R. Durst *et al.*, "Endovascular treatment of ophthalmic artery aneurysms: Ophthalmic artery patency following flow diversion versus coil embolization," *J. Neurointerv. Surg.*, 2016.

[5] C. J. Griessenauer *et al.*, "Pipeline embolization device for small intracranial aneurysms: Evaluation of safety and efficacy in a multicenter cohort," *Neurosurgery*, 2017.

[6] P. Bhogal, O. Ganslandt, H. Bäzner, H. Henkes, and M. A. Pérez, "The Fate of Side Branches Covered by Flow Diverters–Results from 140 Patients," *World Neurosurg.*, 2017.

[7] G. Gascou *et al.*, "Extra-aneurysmal flow modification following pipeline embolization device implantation: Focus on regional branches, perforators, and the parent vessel," *Am. J. Neuroradiol.*, 2015.

[8] C. J. Griessenauer *et al.*, "Flow diverters for treatment of 160 ophthalmic segment aneurysms: Evaluation of safety and efficacy in a multicenter cohort," *Clin. Neurosurg.*, 2017.

[9] R.-C. L. *et al.*, "Patency of anterior circulation branch vessels after Pipeline embolization: Longer-term results from 82 aneurysm cases," *J. Neurosurg.*, 2017.

[10] A. Rouchaud *et al.*, "Visual outcomes with flow-diverter stents covering the ophthalmic artery for treatment of internal carotid artery aneurysms," *Am. J. Neuroradiol.*, 2015.

[11] M. Zanaty *et al.*, "Flow-diversion for ophthalmic segment aneurysms," *Neurosurgery*, 2015.

[12] A. M. Burrows, W. Brinjikji, R. C. Puffer, H. Cloft, D. F. Kallmes, and G. Lanzino, "Flow diversion for ophthalmic artery aneurysms," *Am. J. Neuroradiol.*, 2016.

[13] A. P. Narata *et al.*, "The Role of Hemodynamics in Intracranial Bifurcation Arteries after Aneurysm Treatment with Flow-Diverter Stents," *Am. J. Neuroradiol.*, vol. 39, no. 2, 2018.

[14] C. Iosif *et al.*, "Role of terminal and anastomotic circulation in the patency of arteries jailed by flow-diverting stents: animal flow model evaluation and preliminary results," 2016.

[15] J. R. Cebral *et al.*, "Analysis of hemodynamics and aneurysm occlusion after flow-diverting treatment in rabbit models," *Am. J. Neuroradiol.*, 2014.

[16] R. Bott, *Guyton and Hall Textbook of Medical Physiology 13ed*, no. 1. 2014.

[17] P. Reymond, F. Merenda, F. Perren, D. Rüfenacht, and N. Stergiopulos, "Validation of a one-dimensional model of the systemic arterial tree.," *Am. J. Physiol. Heart Circ. Physiol.*, vol. 297, no. 1, pp. H208-22, Jul. 2009.

[18] M. C. Villa-Uriol *et al.*, "@neurIST complex information processing toolchain for the integrated management of cerebral aneurysms.," *Interface Focus*, vol. 1, no. 3, pp. 308–19, Jun. 2011.

[19] I. Larrabide, M. Kim, L. Augsburger, M. C. Villa-Uriol, D. Rüfenacht, and A. F. Frangi, "Fast virtual deployment of self-expandable stents: Method and in vitro evaluation for intracranial aneurysmal stenting," *Med. Image Anal.*, vol. 16, no. 3, pp. 721–730, 2012.

[20] A. Marzo *et al.*, "Computational hemodynamics in cerebral aneurysms: The effects of modeled versus measured boundary conditions," *Ann. Biomed. Eng.*, vol. 39, no. 2, pp. 884–896, 2011.

[21] A. Marzo, P. Singh, P. Reymond, N. Stergiopulos, U. Patel, and R. Hose, "Influence of inlet boundary conditions on the local haemodynamics of intracranial aneurysms.," *Comput. Methods Biomech. Biomed. Engin.*, vol. 12, no. 4, pp. 431–444, Aug. 2009.

[22] P. Reymond, F. Merenda, F. Perren, D. Rüfenacht, and N. Stergiopulos, "Validation of a one-dimensional model of the systemic arterial tree.," *Am. J. Physiol. Heart Circ. Physiol.*, vol. 297, no. 1, pp. H208-22, 2009.

[23] P. Cignoni, C. Rocchini, and R. Scopigno, "Metro: Measuring Error on Simplified Surfaces," *Comput. Graph. Forum*, 1998.

[24] S. Appanaboyina *et al.*, "Computational modelling of blood flow in side arterial branches after stenting of cerebral aneurysms," *Int. J. Comut. Fluid Dyn.*, 2008.

[25] A. J. Geers, I. Larrabide, H. G. Morales, and A. F. Frangi, "Approximating hemodynamics of cerebral aneurysms with steady flow simulations," *J. Biomech.*, 2014.

[26] H. G. Morales, I. Larrabide, A. J. Geers, M. L. Aguilar, and A. F. Frangi, "Newtonian and non-Newtonian blood flow in coiled cerebral aneurysms," *J. Biomech.*, 2013.

[27] P. Aparício, M. S. Thompson, and P. N. Watton, "A novel chemo-mechano-biological model of arterial tissue growth and remodelling," *J. Biomech.*, 2016.

Dataset	Location	J-Ves Narrowing	J-Vess Diam [mm]	J-Vess R [mmHg s ml^-1]	Periph R [mmHg s ml^-1]	R_{FDS} [mmHg s ml^-1]	$\%R_{FDS}$
1	ICA	NO	1.09	8	470	5	1.04
2	ICA	NO	1.05	10	470	5	1.04
3	ICA	NO	1.08	9	470	5	1.04
4	ICA	NO	1.07	9	470	5	1.04
5	ICA	NO	1.08	9	470	5	1.04
6	ICA	NO	1.16	6	470	5	1.05
7	ICA	NO	1.07	9	470	5	1.04
8	ICA	NO	1.24	5	470	5	1.05
9	ICA	NO	1.06	9	470	5	1.04
10	ICA	NO	1.13	7	470	5	1.05
11	ICA	NO	1.23	5	470	5	1.05
12	ICA	NO	1.09	8	470	5	1.05
13	ICA	NO	1.30	4	470	5	1.05
14	ICA	NO	1.14	7	470	5	1.05
15	ICA	NO	1.11	8	470	5	1.05
16	ICA	NO	1.13	7	470	5	1.05
17	ICA	NO	1.17	6	470	5	1.05
18	ICA	NO	1.21	6	470	5	1.05
19	ICA	NO	1.17	6	470	5	1.05
20	ICA	NO	1.11	8	470	5	1.05
21	ICA	NO	1.15	7	470	5	1.05
22	ICA	NO	1.15	7	470	5	1.05
23	ICA	NO	1.27	5	470	5	1.05
24	ICA	NO	1.15	7	470	5	1.05
25	ICA	NO	1.19	6	470	5	1.05
26	ICA	NO	0.98	13	470	5	1.04
27	ICA	NO	1.10	8	470	5	1.05
28	ICA	NO	1.16	6	470	5	1.05
29	ICA	NO	1.16	7	470	5	1.05
30	ICA	NO	1.19	6	470	5	1.05
31	ICA	NO	1.10	8	470	5	1.05
32	ICA	NO	1.18	6	470	5	1.05
33	ICA	NO	1.14	7	470	5	1.05
34	ICA	NO	1.01	11	470	5	1.04
35	ICA	NO	1.18	6	470	5	1.05
36	ICA	NO	1.17	6	470	5	1.05
37	ICA	NO	1.12	7	470	5	1.05

Table 1 *(online suppl.) Demographic constitution and anatomical data of patients' population. J-Vess Diam = jailed vessel diameter, J-Vess R = jailed vessel vascular resistance, Periph R = peripheral resistance, R_{FDS}= FDS-induced resistance to flow, % R_{FDS}= FDS-induced resistance to flow given as a percentage of overall resistance (FDS plus vascular plus peripheral).*

38	ICA	NO	1.30	4	470	5	1.05
39	ICA	NO	1.14	7	470	5	1.05
40	ICA	NO	1.22	5	470	5	1.05
41	ICA	NO	1.27	5	470	5	1.05
42	ICA	NO	1.07	9	470	5	1.04
43	ICA	NO	1.22	5	470	5	1.05
44	ICA	NO	1.15	7	470	5	1.05
45	ICA	NO	1.23	5	470	5	1.05
46	ICA	NO	1.26	5	470	5	1.05
47	ICA	NO	1.13	7	470	5	1.05
48	ICA	NO	1.08	9	470	5	1.04
49	ICA	NO	1.25	5	470	5	1.05
50	ICA	NO	1.10	8	470	5	1.05
51	ICA	NO	1.25	5	470	5	1.05
52	ICA	NO	1.13	7	470	5	1.05
53	ICA	NO	1.11	8	470	5	1.05
54	ICA	NO	1.10	8	470	5	1.05
55	ICA	NO	1.19	6	470	5	1.05
56	ICA	NO	1.05	10	470	5	1.04
57	ICA	NO	1.12	8	470	5	1.05
58	ICA	NO	1.15	7	470	5	1.05
59	ICA	NO	1.12	8	470	5	1.05
60	ICA	NO	1.09	8	470	5	1.04
61	ICA	NO	1.20	6	470	5	1.05
62	ICA	NO	1.13	7	470	5	1.05
63	ICA	NO	1.17	6	470	5	1.05
64	ICA	NO	1.09	8	470	5	1.05
65	ICA	NO	1.14	7	470	5	1.05
66	ICA	NO	1.00	12	470	5	1.04
67	ICA	NO	1.13	7	470	5	1.05
68	ICA	NO	1.12	8	470	5	1.05
69	ICA	NO	1.14	7	470	5	1.05
70	ICA	NO	1.16	6	470	5	1.05
71	ICA	NO	1.11	8	470	5	1.05
72	ICA	NO	1.12	7	470	5	1.05
73	ICA	NO	1.11	8	470	5	1.05
74	ICA	NO	1.18	6	470	5	1.05
75	ICA	NO	1.13	7	470	5	1.05
76	ICA	NO	1.10	8	470	5	1.05
77	ICA	NO	1.13	7	470	5	1.05
78	ICA	NO	1.05	10	470	5	1.04
79	ICA	NO	1.17	6	470	5	1.05

80	ICA	NO	1.12	7	470	5	1.05
81	ICA	NO	1.14	7	470	5	1.05
82	ICA	NO	1.20	6	470	5	1.05
83	ICA	NO	1.14	7	470	5	1.05
84	ICA	NO	1.05	10	470	5	1.04
85	ICA	NO	1.19	6	470	5	1.05
86	ICA	NO	1.05	10	470	5	1.04
87	ICA	NO	1.14	7	470	5	1.05
88	ICA	NO	1.13	7	470	5	1.05
89	ICA	NO	1.15	7	470	5	1.05
90	ICA	NO	1.05	10	470	5	1.04
91	ICA	NO	1.20	6	470	5	1.05
92	ICA	NO	1.17	6	470	5	1.05
93	ICA	NO	1.12	8	470	5	1.05
94	ICA	NO	1.13	7	470	5	1.05
95	ICA	NO	1.03	11	470	5	1.04
96	ICA	NO	1.16	7	470	5	1.05
97	ICA	NO	1.13	7	470	5	1.05
98	ICA	NO	1.11	8	470	5	1.05
99	ICA	NO	1.11	8	470	5	1.05
100	ICA	NO	1.07	9	470	5	1.04
101	ICA	NO	1.12	8	470	5	1.05
102	ICA	NO	1.17	6	470	5	1.05
103	ICA	NO	1.03	10	470	5	1.04
104	ICA	NO	1.13	7	470	5	1.05
105	ICA	NO	1.16	6	470	5	1.05
106	ICA	NO	1.09	8	470	5	1.05
107	ICA	NO	1.13	7	470	5	1.05
108	ICA	NO	1.17	6	470	5	1.05
109	ICA	NO	1.17	6	470	5	1.05
110	ICA	NO	1.13	7	470	5	1.05
111	ICA	NO	1.14	7	470	5	1.05
112	ICA	NO	1.17	6	470	5	1.05
113	ICA	NO	1.02	11	470	5	1.04
114	ICA	NO	1.13	7	470	5	1.05
115	ICA	NO	1.11	8	470	5	1.05
116	ICA	NO	1.15	7	470	5	1.05
117	ICA	NO	1.11	8	470	5	1.05
118	MCA	YES	1.05	62	75	5	3.66
119	ACOM	YES	1.05	62	75	5	3.66
120	MCA	YES	1.6	11	75	5	5.79
121	MCA	YES	1.05	62	75	5	3.66

122	BA	YES	1.15	43	75	5	4.24
123	MCA	YES	1.04	64	75	5	3.60
124	MCA	NO	1.55	13	75	5	5.68
125	MCA	NO	1.53	14	75	5	5.64
126	MCA	YES	1.2	36	75	5	4.50
127	MCA	NO	2.06	4	75	5	6.32
128	MCA	NO	2.37	2	75	5	6.46
129	MCA	YES	0.83	158	75	5	2.15
130	MCA	NO	1.82	7	75	5	6.11
131	BA	YES	0.75	237	75	5	1.60
132	MCA	YES	1.83	7	75	5	6.12
133	BA	NO	2.08	4	75	5	6.33
134	BA	NO	1.39	20	75	5	5.26
135	MCA	YES	1.04	64	75	5	3.60
136	BA	YES	0.96	88	75	5	3.06
137	BA	NO	1.24	32	75	5	4.69
138	MCA	NO	1.68	9	75	5	5.92
139	MCA	YES	1.1	51	75	5	3.96
140	MCA	YES	1.6	11	75	5	5.79
141	ACOM	NO	1.75	8	75	5	6.03
142	MCA	YES	0.88	125	75	5	2.50

Table 2 Quantification of FDS-induced changes to haemodynamic variables extracted from OphthA bifurcation at peak systole (peak) and end diastole (dia). Avg WSS is the space-averaged WSS extracted from the OphthA. ICA and Ophth outflow are the volumetric flow rates calculated at the outlet of the ICA and OphthA, respectivelty.

	Unstented [peak/dia]	*Stended* [peak/dia]	*Diff* [peak/dia]	*%Diff* [peak/dia]
Avg WSS [Pa]	11.56/5.30	10.98/5.04	-0.58/-0.26	-5.0/-4.7
ICA outflow [ml/s]	7.20/3.80	7.19/3.82	-0.01/-0.02	0.1/0.5
Ophth outflow [ml/s]	0.38/0.20	0.38/0.201	0.0/0.001	0.0/0.5